ChemPubSoc Europe

DOI: 10.1002/batt.201800149

BATTERIES & SUPERCAPS
Articles

Special Issue

The Indium–Lithium Electrode in Solid-State Lithium-Ion Batteries: Phase Formation, Redox Potentials, and Interface Stability

A. L. Santhosha[+],[a, b] Lukas Medenbach[+],[a, b] Johannes R. Buchheim,[a, b] and Philipp Adelhelm*[a, b]

Lithium solid-state batteries (Li-SSBs) require electrodes that provide a sufficiently stable interface with the solid electrolyte. Due to the often limited stability window of solid electrolytes, researchers frequently favor an In–Li alloy instead of lithium metal as counter electrode for two-electrode measurements. Maintaining a stable potential at the counter electrode is especially important because three-electrode measurements are hard to realize in solid-state cells. Although a constant potential of about 0.6 V vs. Li^+/Li is commonly accepted for the In–Li electrode, only little is known about the behavior of this electrode. Moreover, the In–Li phase diagram is complex containing several intermetallic phases/compounds such as the InLi phase, or line compounds such as In_4Li_5 or In_2Li_3. This means that the redox potential of the In–Li electrode depends on the alloy composition, i.e. the In/Li ratio. Here, we study the behavior of In–Li electrodes in cells with liquid electrolyte to determine their phase evolution and several equilibrium potentials vs. Li^+/Li. The room temperature equilibrium redox potential of the In–Li electrode with the favored composition (or more precisely the Li^+/(In–InLi) electrode) is 0.62 V vs. Li^+/Li. We then discuss the use of In–Li electrodes in solid state cells using Li_3PS_4 as solid electrolyte and give examples on the importance of the right In/Li ratio of the electrode. While the right In/Li ratio enables stable lithium insertion/deinsertion in symmetrical cells for at least 100 cycles, too much lithium in the electrode leads to a drop in redox potential combined with a rapid build-up of interface resistance.

1. Introduction

The market of lithium-ion batteries (LIBs) is rapidly increasing and the continuous development in portable electronics and in the mobility sector requires further improvements of this technology.[1] A critical component of LIBs is the liquid organic electrolyte, which is highly flammable and possesses a safety risk. Further improvements therefore might require a conceptual change away from the classical cell design. The currently most intensively investigated strategy is the solid-state-battery (SSB) approach, implemented by replacing the flammable liquid electrolyte by nonflammable, inorganic solids with high ionic conductivity. Besides better safety, there is also hope that the SSB concept eases a bipolar cell stack design or enables the use of a lithium metal anode, both leading to increase in energy density and power density.[2]

In this account, recent efforts aim at finding and developing suitable solid electrolytes (SE) that are mechanically and (electro-)chemically stable, exhibit a high ionic conductivity (preferably $> 10^{-3}$ S cm^{-1}) and that can be produced at low cost.[3] One can distinguish Li-ion conducting SE's in either oxidic type ceramics or sulfidic type glasses and glass-ceramics. LISICON or Li-garnets like LLZO are well investigated representatives of oxidic SE's having good ionic conductivity in range of 10^{-3} S cm^{-2}[4] A common challenge for oxides is the need of high sintering temperatures to overcome detrimental grain boundary resistance and poor particle-particle contact.[5] Sulfide based SE's, on the other hand, emerged more recently as class of superionic solid Li-ion conductors, which can be synthesized at lower temperature and, thanks to their softness, promise negligible grain boundary resistance as they can be compacted by simple cold pressing. In this regard, the highest ionic conductivity of 12 mS cm^{-1} has been reported for $Li_{10}GeP_2S_{12}$,[6] a member of the auspicious thiophosphate SE class current research is focusing on.[7] An important challenge of these electrolytes is the moisture sensitivity which complicates the handling and processing. A concern to all solid electrolytes is the (electro-) chemical stability against electrode materials.[8] Although better stability over liquid electrolytes is frequently mentioned, it is important to realize that this is not necessarily the case. For example, Richards *et al.* calculated the thermodynamic electrochemical stability window for a variety of electrolytes showing that especially the thiophosphates can be easily reduced or oxidized.[9] Several experimental reports indicate that physical contact between lithium metal and thiophosphate

[a] A. L. Santhosha,[+] L. Medenbach,[+] Dr. J. R. Buchheim, Prof. Dr. P. Adelhelm
Institute of Technical Chemistry and Environmental Chemistry
Friedrich Schiller University Jena
Philosophenweg 7a, 07743 Jena, Germany
E-mail: philipp.adelhelm@uni-jena.de
[b] A. L. Santhosha,[+] L. Medenbach,[+] Dr. J. R. Buchheim, Prof. Dr. P. Adelhelm
Center for Energy and Environmental Chemistry Jena (CEEC Jena)
Friedrich Schiller University Jena
Philosophenweg 7a, 07743 Jena, Germany
[+] These authors contributed equally to this work

Supporting information for this article is available on the WWW under https://doi.org/10.1002/batt.201800149

Special Issue An invited contribution to a Special Issue on SEI and Interphases at Electrodes

SE's leads to the formation of Li_3P, Li_2S and other side products at the Li–SE interface.[10,4b] Hence, impedance increases and as a result fast cell degradation occurs.[11]

Due to this problem, lithium alloys are investigated. These can be often easily synthesized by solid state diffusion at ambient temperature. Especially lithium intermetallic phases containing Al, Ga, In, Sn or Sb can possess even larger chemical diffusion coefficients when compared with the Li-self-diffusion.[12] Insertion of lithium into metals (i.e. alloy formation) typically occurs at potentials below ~1 V vs. Li^+/Li. This is still outside the limit for thiophosphate electrolytes.[9] However, the thermodynamic driving force for electrolyte reduction is lowered compared to lithium metal. Because of this, the use of lithium alloys instead of lithium metal is currently an attractive route to reach a more stable electrode/solid electrolyte interface that enables long-term cycling of solid state batteries (unless their redox potential becomes not too high).[13] The use of an alloy instead of Li would also miminize the issue of dendrite formation and hence would eliminate the risk of short circuiting.[9] Despite the risk of dendrite formation, one has to mention that interfaces between Li and selected solid electrolytes can be "stable". Such situations are found for LiPON[14] and cubic $Li_{7-3x}Al_xLa_3Zr_2O_{12}$[15] for which extremely thin interphases form in contact with lithium. However, these solid electrolytes have their own limitations. LiPON is a thin film solid electrolyte and c-LLZO is a complex and mechanically hard material that requires high synthesis temperatures.

Among the variety of lithium alloys, the indium–lithium (In–Li) system is particularly popular.[16] The high cost of indium impedes any large-scale application; however, its high ductility is of great advantage for assembling laboratory solid state cells and the alloy can provide a constant redox potential of about 0.6 V vs. Li^+/Li (0.5 V at 415 °C)[17] over a wide stoichiometry range.[18–19] The use of indium therefore provides a convenient route for assembling SSBs and hence enables electrochemical studies on materials and electrolytes that would otherwise be much more difficult or impossible. Note that the cell assembly of SSBs is currently still much more cumbersome compared to cells with liquid electrolyte as many practical parameters (pressure, grinding, amounts of material etc.) have to be optimized and the solid electrolyte is not commercially available. Moreover, it is very difficult to insert a reference electrode to SSBs which underlines the need for a counter electrode with stable potential (here the alloy).

In this study we focus on the In–Li binary system as electrode for SSBs. Firstly, we determine the redox potentials of lithium insertion into indium at room temperature by coulometric titration technique using a liquid electrolyte. We show that at room temperature Li and In are able to form different intermetallic phases/compounds in accordance with known binary phase diagram. Secondly, we study the interface stability of In–Li electrodes in symmetric solid-state cells. As solid electrolyte we chose β-Li_3PS_4 as representative for the thiophosphate SE class. We show that the stability between SE and the In–Li electrode strongly depends on the stoichiometry of the intermetallic phase. These measurements clearly indicate that adjusting the right stoichiometry of the In–Li electrode is crucial for obtaining (improved) stability toward the solid electrolyte.

Experimental Section

Coulometric titration of indium by lithium was done to follow the formation of different intermetallic phases of the binary In/Li phase diagram. For this, a Swagelok-type 3-electrode cell with liquid electrolyte was used. An indium disc (d = 12 mm, thickness = 0.125 mm, m ≈ 120 mg, Chempur 99.99%) was connected as working electrode, whereas lithium (Rockwood Lithium, 99.8%) was used as counter electrode (d = 12 mm, thickness = 0.5 mm) and reference electrode, respectively. A 1 M solution of lithium bis (trifluoromethanesulfonyl)imide (LiTFSI„ Sigma Aldrich, >98%) dissolved in a 1:1 mixture of dioxolane (DOL, Sigma Aldrich) and dimethoxyethane (DME, Sigma Aldrich) was used as electrolyte. All solvents were dried for 24 h in molecular sieve (4 Å). LiTFSI was used as received. The cell assembly was carried out in an argon filled glovebox (MBraun; O_2 < 0.1 ppm and H_2O < 0.1 ppm). Galvanostatic lithiation was conducted using Bio-Logic MPG2 multichannel cycler. The measurement consisted of several 1 h current pulses (≈280 μA cm^{-2}) each followed by a 0.5 h rest period for obtaining the open circuit voltage (OCV). The impedance measurements were performed in the frequency range from 1 MHz to 0.1 Hz with a potential amplitude of 10 mV. Impedance spectra fitting was done with *RelaxIS 3* software (*rhd instruments*). All electrochemical experiments were performed at room temperature. The X-ray diffraction (XRD) measurements are performed on a Bruker PhaserD2 diffractometer using Cu Kα (λ = 1.5406 Å) radiation and a 2θ angle range from 10° to 60°. Measurements were done after removing the electrodes (from cells with liquid electrode) using a protective XRD sample holder to prevent air contact.

The thiophosphate SE (β-Li_3PS_4) was synthesized by a solvent method followed by heat treatment similar to ref. [7b] (supporting information-1). Preparation of solid-state cells was performed by cold pressing of 100 mg SE inside a uniaxial cylinder cell (3 tons for 3 minutes, 10 mm diameter) followed by pressing an indium disc and subsequently a lithium disc on both sides, respectively. Two different In:Li ratios were investigated: 4 mg Li (d = 10 mm, thickness = 0.12 mm) combined with 84 mg In (1.27 In:Li) and 15 mg Li (d = 10 mm, thickness = 0.5 mm) combined with 84 mg In (0.34 In:Li). Solid electrolyte synthesis and solid-state cell construction were carried out inside an argon filled glove box (MBraun; O_2 < 0.1 ppm and H_2O < 0.1 ppm). Galvanostatic Li insertion/deinsertion (1 mA cm^{-2}) was done at room temperature using Biologic MPG2 cycler.

2. Results and Discussion

2.1. The In–Li Electrode with Liquid Electrolyte: Phase Diagram and Determination of Redox Potential versus Li^+/Li

The In/Li binary phase diagram is shown in Figure 1. Starting from pure In (left, 0 at%), the system passes alternately through one- and two-phase regions finally ending on the pure Li side (right, 100 at%). The intermetallic phases are InLi, In_4Li_5, In_2Li_3, $InLi_2$, $InLi_3$ and In_3Li_{13}. Interestingly, only the InLi phase shows an extended homogeneity range reaching up to about 20 at% towards the Li-rich side at elevated temperature. The other intermetallic phases (line compounds) as well as the solid solutions (In) and (Li) of the end members have a very narrow

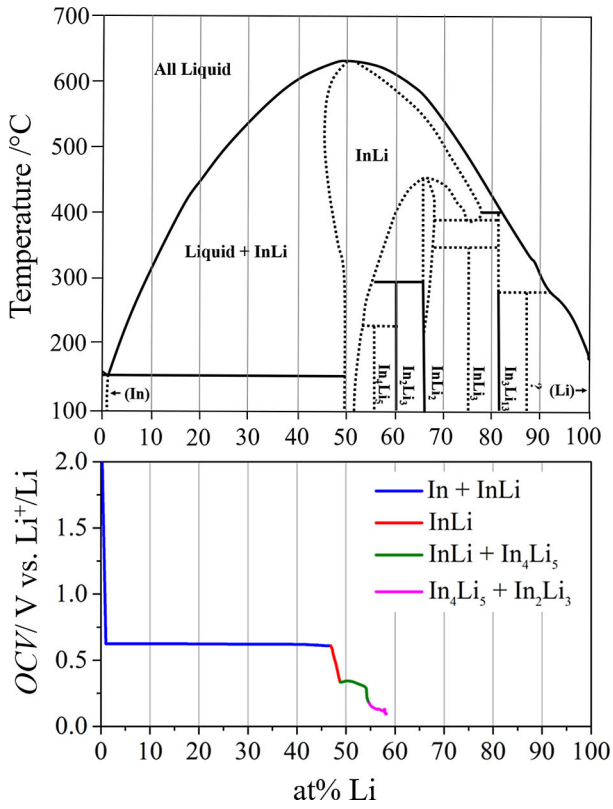

Figure 1. Top: Binary In–Li phase diagram (redrawn from reference [9a]). Bottom: Results from a coulometric titration experiment at room temperature. The graph shows the electrochemically determined open circuit voltage (OCV) over the lithiation of In until the phase In_2Li_3. Note that the scale of the x-axis (lithium content) is identical for both graphs.

stability range at all temperatures (note that the brackets for (In) and (Li) are used to indicate the solid solution phase, which is, however, extremely small for both metals). Although the diagram represents the phase behavior for elevated temperatures $>100\,^{\circ}C$ and is not fully confirmed (dotted lines), it is a good starting point for predicting the behavior at room temperature.

From a thermodynamic point of view, we can directly predict the shape of the potential profile (relaxed state) from the phase diagram:

- *Two phase region*: Inside the two phase region, the lithium activity *a* in both phases is constant. Therefore, the chemical potential μ and hence the potential are constant.
- *One phase region*: Inside the one phase region, the lithium activity *a* changes due to $\mu = \mu_0 + R \cdot T \cdot \ln(a)$ and therefore a sloping potential is observed.

As the homogeneity ranges of (In), (Li) and the intermetallic compounds are negligible at room temperature, the phase diagram is dominated by two-phase regions and therefore electrochemical lithiation of indium should lead to several consecutive steps with voltage plateaus in between. The only exception being the homogeneity range of the InLi phase where a sloping potential is expected.

The electrochemical lithiation of In can be understood as coulometric titration (with only solid phases) with the lithium content being sequentially increased. Each lithiation step (at constant current) is followed by a relaxation step of 0.5 h. After relaxation, the OCV value is collected. Thus, the method does not only deliver precise information on the phase diagram, it also provides thermodynamic data on the Gibbs energies of the different reactions. Figure 1 bottom displays the OCV values for different lithium contents. As the OCV and the number of transferred electrons per reaction equivalent (*z*) are both given by this experiment, the thermodynamic driving force $\Delta_r G$ for each reaction step can be simply calculated by equation 1.

$$\Delta_r G = -z \cdot F \cdot OCV \qquad (1)$$

The profile starts with a long plateau at 0.62 V corresponding to the formation of the InLi intermetallic phase from Li and In, which results in a $\Delta_f G$-value of $-57\ kJ\,mol^{-1}$ (we neglect the very small homogeneity range of the (In) solid solution).

$$In + Li^+ + e^- \rightarrow InLi$$

This is followed by a short, largely linear sloping behavior for the homogeneity range of the InLi phase ($\Delta x_{Li} \approx 1.9$ at%). Subsequently, two more plateaus occur representing the formation of In_4Li_5 (~0.34 V, $-8.7\ kJ\,mol^{-1}$) and In_2Li_3 (~0.12 V, $-3.4\ kJ\,mol^{-1}$), respectively.

We stopped the experiment at a lithium content of 60% (with In_2Li_3 as final phase). Our efforts for deeper lithiation were not successful. This is likely due to the decreasing thermodynamic driving force with redox potentials approaching 0 V vs. Li^+/Li. In our measurements, the cut-off potential of 0.01 V vs. Li^+/Li was therefore reached even by small kinetic barriers. Overall, the electrochemical data is matching well with the binary phase diagram and we confirmed the lithiation of the In electrode indicating rapid solid state diffusion. However, we note the minor discrepancy that the onset of the InLi-phase is already at 47% and ends at 49%. This indicates that a minor amount of indium was not lithiated in the electrode possibly related to local decontacting due to the volume expansion. According to the densities of the different phases, one can estimate a volume expansion of about 53% for the formation of the InLi phase (pdf 98-005-1959).

A more detailed view is provided in Figure 2a which shows the potential over time for the consecutive lithiation/relaxation steps. This readily provides information on degree of overpotentials over time for the different regions. At the beginning, the overpotential is in the range of about 0.10 V. Values decrease in the following current pulses to a minimum of 0.04 V but then increase again and remain at about 0.10 V until the formation of InLi phase is completed. Interestingly, the overpotential for the formation of In_4Li_5 from the InLi phase at the second plateau is somewhat smaller (~0.06 V), which indicates less limited reaction conditions.

These observations were confirmed by electrochemical impedance spectroscopy (PEIS) conducted at selected states of lithiation (Figure 2b). The impedance behavior is interpreted using an equivalent circuit model consisting out of two parallel *R*/*CPE*-elements, each attributed to an interfacial process and a

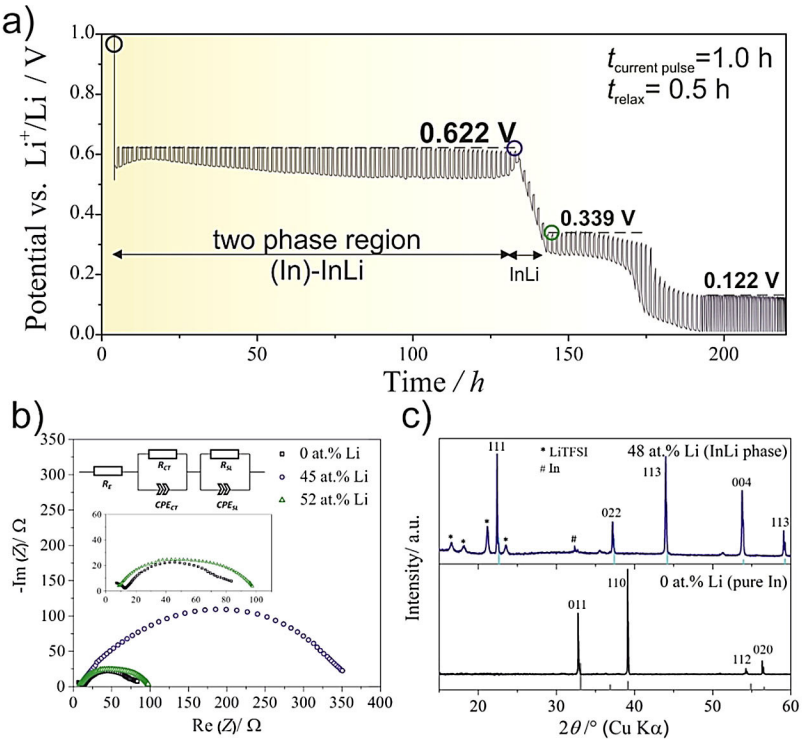

Figure 2. a) Potential profile during lithiation on indium over time for consecutive current (200 μA/cm^2 or 2350 μA/g) and relaxation steps. The graph shows the equilibrium potentials for the different plateaus. b) The circles indicate the position at which impedance spectra were collected, electrochemical impedance spectra (1 MHz–100 mHz) at different degrees of lithiation. Fitting results are available in supporting information Table S1–S3. c) XRD patterns of indium metal and after reaching the end of the first plateau. The XRD patterns are in accordance with the reference patterns (In: pdf 98-006-3091, InLi: pdf 98-005-1959).

further resistance whichlargely represents ion transport in bulk electrolyte (R_E). Before lithiation (0 at% Li) no solid electrolyte interphase formation is expected and the main impedance signal should be dominated by charge transfer at the electrode electrolyte interface (R_{CT}/CPE_{CT}). Our measurement exhibits two semicircles, one at high frequency range and another one at intermediate frequency range (119 Hz). Because it can be extrapolated to 0 we attribute the smaller signal to the electrolyte phase impedance. In this case, the imaginary part arises from charge separation inside the bulk electrolyte induced by frequencies in the MHz range. Taking this into account, we conclude that the second signal must represent the Li^+— charge transfer process.

A second measurement was conducted at a Li content of 45 at%, i.e. close to the end of the first plateau region (Figure 1). The total impedance raised by a factor of 4–5 which explains the higher overpotentials observed. In this case, the contribution of an SEI has to be considered as well, so the spectrum shows a combination of surface layer impedance (R_{SL}/CPE_{SL}) and charge transfer impedance. As discussed in literature, surface layer impedance is measured in the higher frequency range so we attribute the smaller shoulder of the spectrum to the SEI, which was formed during lithiation.[20] Hence, for the given degree of lithiation, the impedance behavior seems to be still dominated by charge transfer taking place at much higher resistance. Considering InLi as sole possible product in the applied potential range, we think that the low remaining amount of In might be responsible for higher charge transfer resistance.

With a Li percentage of 52 at% the system is located in second plateau region. R_{SL} and R_{CT} decreased back to 100 Ω in sum indicating faster reaction kinetics for InLi–In_4Li_5 phase (0.34 V vs. Li^+/Li). Both, lower potential and faster kinetics, might enhance possible degradation reactions reported for solid electrolytes (See also Figure S2).

Ex situ XRD measurements were conducted to confirm the formation of the InLi phase at the end of the voltage plateau region (0.62 V), see Figure 2c. The Bragg positions confirm a cubic unit cell with space group *F*d3m (PDF 09-0066). Besides InLi, also some minor amount of non-reacted indium metal is detected. The presence of some indium metal is in line with the slightly earlier completion of InLi-phase formation (47%–49%) as already mentioned above.

At this point, it is important to note that it was generally challenging to obtain reliable data. Although we always found the same trend in data, lithiation of indium in cells with liquid electrolyte is generally difficult and experimental data scatters. This indicates a very unstable interface/interphase between the electrode and the liquid electrolyte. For example, all our attempts for using a carbonate based electrolyte (EC:DMC 1:1) were unsuccessful. This finding is in line with results from Webb *et al.*[19] on sputtered indium thin films (d≈3 μm). Using a carbonate electrolyte ($LiPF_6$ in EC:DMC), they could only lithiate indium by adding larger amounts of FEC additive (which still

did not lead to a stable SEI). This likely explains the lack of data on the electrochemical lithiation of indium at room temperature. Besides high temperature measurements by Wen and Huggins,[17] our study and the one by Webb *et al* are, to the best of our knowledge, the only ones studying the lithiation of indium at room temperature. In view of this and despite the challenges encountered, our study nevertheless suggested that ethers (in our case DOL/DME as 1:1 solvent mixture) are preferable solvents for lithiating indium. We also determined the room temperature equilibrium redox potential of the In–Li electrode (or more precisely the Li^+/(In–InLi) electrode) to 0.62 V vs. Li^+/Li.

2.2. The In–Li Electrode with Solid Electrolyte – Relevance of Mass Balancing

The results from the previous section show that the electrochemical lithiation of a bulk indium foil up to phases having potentials close to Li metal is possible at room temperature and at reasonable currents. Hence, this suggests that the same phases or such with even higher lithium content can form by simply bringing both metals in direct physical contact. This is the case when preparing In–Li electrodes by pressing a lithium and indium foil together as it is done for solid-state batteries. Moreover, results from Figure 1 and 2 clearly show that the preferential composition of the In–Li electrode is the two-phase region (In)–InLi, so a careful mass balancing has to be done in order to provide a stable redox potential (0.62 V vs. Li^+/Li) over a large stoichiometric window.

To demonstrate the importance of the right composition for the interface stability, we prepared symmetric solid-state cells and conducted galvanostatic Li^+ insertion/deinsertion experiments (1 mA cm^{-2}). β-Li_3PS_4 was chosen as model solid electrolyte (SE), as it is frequently applied in solid state battery research, see ref. [4b] for example. The SE was synthesized by a solution based method and showed a specific room temperature ionic conductivity of $1.2 \cdot 10^{-4}$ S cm^{-1} as determined by impedance spectroscopy (more information can be found in the supporting information S1). Results for two different In–Li electrodes are shown in Figure 3. In the first case, a lithium (4 mg) and indium foil (84 mg) were combined with the nominal In:Li atomic ratio of 1.26:1. With 44 at% Li, the composition of the electrode is in the two-phase region (In)–InLi. As can be seen, Li^+ insertion/deinsertion could be performed with overpotentials as low as 12 mV. Moreover, no significant change was observed for over 100 cycles (200 h). These results indicate that the In–Li electrode exhibits good charge transfer kinetics as well as sufficient chemical stability toward the solid electrolyte (over the course of the experiment). The calculated total areal resistance of the cell after 100 cycles (200 h) is about 12 Ω cm^2.

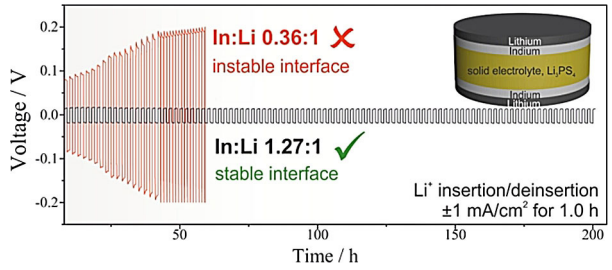

Figure 3. Symmetrical solid-state cells with In–Li electrodes of different stoichiometry and Li_3PS_4 as solid electrolyte. For In–Li compositions within the two-phase region (In)–InLi, Li^+ can be reversibly inserted/deinserted into the electrodes at low overpotentials for many cycles (stable interface, black curve). On the other hand, too high lithium contents (red curve) lead to poor interface stability and hence large polarization and increasing resistance.

In the second case, the lithium content of the In–Li electrode was much higher. A 15 mg lithium foil was combined with a 84 mg indium foil, which corresponds to nominal In:Li atomic ratio of 0.34:1. With almost 75 at% Li, the composition of the electrode is in the two-phase region $InLi_2$–$InLi_3$. In this case, the redox potential is very close to lithium metal, at least $<$0.2 V (see Figure 1). The consequences of this are shown by the red curve in Figure 3. Li^+ insertion/deinsertion of lithium is still possible yet but the polarization becomes much stronger and increases over time. Starting with already higher overpotentials of about 80 mV the value increased up to 200 mV in less than 2 days. Total areal resistance of the cell after this time was about 200 Ω cm^2, i.e. more than 15 times higher compared to the former electrode composition. Results for a third composition (0.81 In:Li) are available in supporting information, see Figure S2.

These results clearly demonstrate that staying in the (In)–InLi plateau region of the phase diagram is very important for conducting SSB experiments. This is not only relevant for maintaining a stable redox potential over a large variation in lithium content but also to maintain good charge transfer kinetics. Wrong mass balancing on the other hand does easily lead to problems. For too high lithium contents, the redox potential might become too low leading to instability with solid electrolytes and therefore increasing interface resistance. Moreover, due to the numerous phases present in the lithium rich region of the phase diagram, the redox potential might easily change when inserting/deinserting lithium ions which complicates the analysis of voltage profiles. Examples of a solid-state cell with CuS as positive electrode and In–Li electrodes of different stoichiometry as negative electrodes are shown in the supporting information, see Figure S3. When using the preferred composition of the In–Li electrode, smaller overpotentials and higher utilization are typically found. A more comprehensive study on the use of CuS in solid-state batteries will be part of a forthcoming study.

3. Conclusion

We studied some fundamental properties of the In–Li electrode in electrochemical cells with liquid and solid electrolyte. Using a liquid electrolyte and hence being able to use a 3-electrode cell with a lithium reference electrode, we followed the phase formation during lithiation of indium. The electrochemical lithiation of a bulk In-disc (120 mg) was possible up to a Li-

content of 60 at%, i.e. formation of In_2Li_3. Overall, our results from the electrochemical lithiation of indium are largely in accordance with the (high temperature) In–Li phase diagram. Different phases can be distinguished in the potential profile as each potential plateau corresponds to a 2-phase region in the binary phase diagram. The stability of the In–Li electrode in cells with liquid electrolytes was comparably poor. Nevertheless, with DOL/DME as electrolyte solvents, we were able to determine the room temperature equilibrium potential of the In–Li electrode within the (In)–InLi two phase region to 0.62 V vs. Li^+/Li. According to our measurements, the homogeneity range of the InLi phase at room temperature is about $\Delta x \approx$ 1.9 at%. Upon lithiation, the redox potential within this phase decreases by about 280 mV. The lithiation reaction and the charge transfer are relatively fast, making the In–Li electrode an attractive counter/reference electrode for SSBs that are commonly two-electrode cells (due to the difficulty in incorporating a reference electrode). For this, however, the mass balancing is crucial as we demonstrated using symmetrical solid-state cells with Li_3PS_4 as model solid electrolyte. As long as the composition of the In–Li electrode is within the two phase region (In)–InLi, reversible Li^+ insertion/deinsertion is possible with only 12 mV of overpotentials at a current density of 1 mA cm^{-2}. For too high lithium contents, however, the chemical stability toward the solid electrolyte is poor resulting in a fast increase in interface resistance upon Li^+ insertion/deinsertion. Our results therefore highlight the importance of adjusting the right In:Li ratio when assembling solid state batteries. The arguments we discussed are valid for any other alloy intended to substitute pure metals (Li, Na) in electrochemical cells. Considering the related alloy phase diagrams is therefore essential for fabricating electrodes with stable interface and redox potential.

Acknowledgements

A.L.S. and P.A. thank for fruitful discussion within the project "FELIZIA" funded by the Federal Ministry of Education and Research (BMBF, grant number 03XP0026I). L.M., J.B. and P.A. thank for support from the Federal State of Thuringia and the European Social Fund (ESF) within the ProExzellenz program and the Forschergruppe Hy-NIB (ENREF 2017 FGR 0055).

Conflict of Interest

The authors declare no conflict of interest.

Keywords: Electrode potentials · Li-alloy anodes · Li_3PS_4 · Solid electrolyte stability · Sulfide solid electrolytes

[1] a) J.-M. Tarascon, M. Armand, *Nature* **2001**, *414*, 359–367; b) J. B. Goodenough, K. S. Park, *J. Am. Chem. Soc.* **2013**, *135*, 1167–1176; c) F. Cheng, J. Liang, Z. Tao, J. Chen, *Adv. Mater.* **2011**, *23*, 1695–1715.

[2] a) R. Koerver, F. Walther, I. Aygün, J. Sann, C. Dietrich, W. G. Zeier, J. Janek, *J. Mater. Chem. A* **2017**, *5*, 22750–22760; b) W. Zhang, D. A. Weber, H. Weigand, T. Arlt, I. Manke, D. Schroder, R. Koerver, T. Leichtweiss, P. Hartmann, W. G. Zeier, J. Janek, *ACS Appl. Mater. Interfaces* **2017**, *9*, 17835–17845; c) A. Sakuda, A. Hayashi, M. Tatsumisago, *Chem. Mater.* **2010**, *22*, 949–956.

[3] a) Y. Wang, W. D. Richards, S. P. Ong, L. J. Miara, J. C. Kim, Y. Mo, G. Ceder, *Nat. Mater.* **2015**, *14*, 1026–1031; b) F. Han, Y. Zhu, X. He, Y. Mo, C. Wang, *Adv. Energy Mater.* **2016**, *6*, 1501590; c) S. Wenzel, D. A. Weber, T. Leichtweiss, M. R. Busche, J. Sann, J. Janek, *Solid State Ionics* **2016**, *286*, 24–33.

[4] a) S. Ohta, T. Kobayashi, T. Asaoka, *J. Power Sources* **2011**, *196*, 3342–3345; b) Z. Zhang, Y. Shao, B. Lotsch, Y.-S. Hu, H. Li, J. Janek, L. F. Nazar, C.-W. Nan, J. Maier, M. Armand, L. Chen, *Energy Environ. Sci.* **2018**, *11*, 1945–1976.

[5] a) R. H. Basappa, T. Ito, T. Morimura, R. Bekarevich, K. Mitsuishi, H. Yamada, *J. Power Sources* **2017**, *363*, 145–152; b) D. O. Shin, K. Oh, K. M. Kim, K.-Y. Park, B. Lee, Y.-G. Lee, K. Kang, *Sci. Rep.* **2015**, *5*, 18053.

[6] N. Kamaya, K. Homma, Y. Yamakawa, M. Hirayama, R. Kanno, M. Yonemura, T. Kamiyama, Y. Kato, S. Hama, K. Kawamoto, A. Mitsui, *Nat. Mater.* **2011**, *10*, 682–686.

[7] a) A. Kuhn, V. Duppel, B. V. Lotsch, *Energy Environ. Sci.* **2013**, *6*, 3548–3552; b) Z. Liu, W. Fu, E. A. Payzant, X. Yu, Z. Wu, N. J. Dudney, J. Kiggans, K. Hong, A. J. Rondinone, C. Liang, *J. Am. Chem. Soc.* **2013**, *135*, 975–978; c) Y. Seino, T. Ota, K. Takada, A. Hayashi, M. Tatsumisago, *Energy Environ. Sci.* **2014**, *7*, 627–631.

[8] P. Hartmann, T. Leichtweiss, M. R. Busche, M. Schneider, M. Reich, J. Sann, P. Adelhelm, J. Janek, *J. Phys. Chem. C* **2013**, *117*, 21064–21074.

[9] W. D. Richards, L. J. Miara, Y. Wang, J. C. Kim, G. Ceder, *Chem. Mater.* **2016**, *28*, 266–273.

[10] a) D. Y. Oh, Y. E. Choi, D. H. Kim, Y.-G. Lee, B.-S. Kim, J. Park, H. Sohn, Y. S. Jung, *J. Mater. Chem. A* **2016**, *4*, 10329–10335; b) S. Teragawa, K. Aso, K. Tadanaga, A. Hayashia, M. Tatsumisago, *J. Mater. Chem. A* **2014**, *2*, 5095–5099.

[11] a) S. Wenzel, T. Leichtweiss, D. A. Weber, J. Sann, W. G. Zeier, J. Janek, *ACS Appl. Mater. Interfaces* **2016** *8*, 28216–28224; b) R. Garcia-Mendez, F. Mizuno, R. Zhang, T. S. Arthur, J. Sakamoto, *Electrochim. Acta* **2017**, *237*, 144–151; c) W. D. Richards, L. J. Miara, Y. Wang, J. C. Kim, G. Ceder, *Chem. Mater.* **2015**, *28*, 266–273; d) Y. Zhu, X. He, Y. Mo, *ACS Appl. Mater. Interfaces* **2015**, *7*, 23685–23693; e) C. Dietrich, D. A. Weber, S. J. Sedlmaier, S. Indris, S. P. Culver, D. Walter, J. Janek, W. G. Zeier, *J. Mater. Chem. A* **2017**, *5*, 18111–18119.

[12] a) J. Sangster, D. Pelton, *J. Phase Equilib.* **1991**, *12*, 37–41; b) Eddie C. Gay, Donald R. Vissers, Fredric J. Martino, Karl E. Anderson, *Journal of electrochemical socity* **1976**, 1591–1596.

[13] D. Y. Oh, Y. E. Choi, D. H. Kim, Y.-G. Lee, B.-S. Kim, J. Park, H. Sohnd, Y. S. Jung, *J. Mater. Chem. A* **2016**, *4*, 10329–10335.

[14] A. Schwöbel, R. Hausbrand, W. Jaegermann, *Solid State Ionics* **2015**, *273*, 51–54.

[15] C. Ma, Y. Cheng, K. Yin, J. Luo, A. Sharafi, J. Sakamoto, J. Li, K. L. More, N. J. Dudney, M. Chi, *ACS Nano letters* **2016**, *16*, 7030–7036.

[16] a) M. Nagao, A. Hayashi, M. Tatsumisago, *Electrochemistry* **2012**, *80*, 734–736; b) S. Wenzel, S. Randau, T. Leichtweiß, D. A. Weber, J. Sann, W. G. Zeier, J. Janek, *Chem. Mater.* **2016**, *28*, 2400–2407; c) J. Lau, R. H. DeBlock, D. M. Butts, D. S. Ashby, C. S. Choi, B. S. Dunn, *Advance energy materials* **2018**, 1800933.

[17] C. J. Wen, R. A. Huggins, *Mater. Res. Bull.* **1980**, *15*, 1225–1234.

[18] K. Takada, N Aotani, K. Iwamoto, S. Kondo, *Solid State Ionics* **1996**, *86–88*, 877–882.

[19] S. A. Webb, L. Baggetto, C. A. Bridges, G. M. Veith, *J. Power Sources* **2014**, *248*, 1105–1117.

[20] a) C. Wang, A. J. Appleby, F. E. Little, *J. Power Sources* **2001**, *93*, 174–185; b) P. G. Bruce, M. Y. Saidi, *J. Electroanal. Chem.* **1992**, *322*, 93–105; c) D. Aurbach, K. Gamolsky, B. Markovsky, Y. Gofer, M. Schmidt, U. Heider, *Electrochim. Acta* **2002**, *47*, 1423–1439.

Manuscript received: December 21, 2018
Revised manuscript received: February 22, 2019
Accepted manuscript online: February 25, 2019
Version of record online: March 26, 2019